On Modeling of Chemical Stimulation of an Enhanced Geothermal System using a High pH Solution with Chelating Agent

Tianfu Xu[1], Peter Rose[2], Scott Fayer[2], and Karsten Pruess[1]

[1]Earth Sciences Division, Lawrence Berkeley National Laboratory, 1 Cyclotron Road, Berkeley, CA 94720
e-mail: Tianfu_Xu@lbl.gov

[2]Energy and Geoscience Institute at the University of Utah • 423 Wakara Way suite 300 Salt Lake City, UT 84108

Abstract. Dissolution of silica and calcite in the presence of a chelating agent (NTA) at a high pH was successfully demonstrated in laboratory experiments using a high-temperature flow reactor. (Note that the term "silica" used here includes amorphous silica, quartz, and silicate glass bead). The mineral dissolution and associated porosity enhancement in the experiments were reproduced by reactive transport modeling using TOUGHREACT. The chemical stimulation method was applied by numerical modeling to a field geothermal injection well system to investigate its effectiveness. Parameters applicable to the quartz monzodiorite unit at the Enhanced Geothermal Systems (EGS) site at Desert Peak (Nevada) were used. Results indicate that the injection of a high pH chelating solution results in dissolution of both calcite and plagioclase, while avoiding precipitation of calcite at high temperature conditions. Consequently reservoir porosity and permeability can be enhanced especially near the injection well. Injection at a lower temperature of 120 ^{o}C (over 160^{o}C in the base-case) results in a porosity increase that is smaller close to the injection point, but extends to a larger radial distance. A slower kinetic rate results in less aggressive mineral dissolution close to the injection point and larger extent along the flow path, which is favorable for chemical stimulation.

Key words. chemical stimulation, high pH solution, chelating agent, Enhanced Geothermal System, EGS, Desert Peak.

1. Introduction

The U.S. Department of Energy (DOE) has broadly defined enhanced (or engineered) geothermal systems (EGS) as engineered reservoirs that have been created to extract economical amounts of heat from geothermal resources of low permeability and/or porosity (Masschusetts Institute of Technology: MIT, 2006). The MIT report indicated that EGS could become a major supplier of primary energy for U.S. base-load generation, with capacity as high as 100,000 MW (electric) by 2050.

The most crucial step in developing EGS for commercial production is "reservoir stimulation," a process that involves injecting fluids under high pressure through boreholes deep underground, with the objective of increasing in situ fluid pressures to the point where effective normal stress on pre-existing rock fractures becomes small or negative. This will create favorable conditions for fractures to "fail in shear," meaning that one or both fracture surfaces will experience translational motion, creating a mismatch between rough surfaces that will enhance reservoir porosity and permeability.

In the early days of EGS research (1980-90s), the focus in reservoir stimulation had been almost exclusively on the geomechanical aspects of manipulating effective stress to enhance fracture permeability. Research into EGS field systems in different countries has gradually led to the recognition that chemical interactions between injected fluids and rocks can be as important as mechanical ones. Stimulation fluids used in EGS development typically are aqueous-based because water is a powerful ionic solvent, especially at higher temperatures. Accordingly, aqueous-based reservoir stimulation is likely to promote dissolution of some rock minerals, while precipitating others, with large impacts on the permeability of the fracture network, and the rate at which fluids can be circulated to bring usable heat to the land surface. The chemical interactions between rocks and fluids must be understood and reliably predicted, in order that stimulation treatments can be properly planned and executed.

The conventional method for chemically removing silica minerals is through mineral acid (such as HCl) treatments, which are expensive and hazardous. Laboratory experiments indicate, however, that aqueous solutions at high pH can dissolve wellbore silica and near-wellbore formation silica and quartz reasonably well and at much lower

cost than HCl treatments (Rose et al., 2007). What has prevented geothermal operators from using caustic solutions in the past is the fear of calcite deposition, which is strongly favored at high pH. The laboratory studies (Mella et al., 2006) have indicated that calcite is dissolved rather than precipitated at high pH in the presence of a chelating agent. This suggests that thermally stable chelating agents at high pH can provide the basis for an economical and effective mineral dissolution approach.

In this paper, we first discuss the principle of calcite dissolution using chelating agents. Then, we present results of calcite and silica dissolution and porosity enhancement in laboratory experiments, and the calibration of a dissolution model by reactive transport modeling using the TOUGHREACT code. Finally, we present applications of this chemical stimulation method to a geothermal injection well system using a mineralogical composition from the Desert Peak (Nevada) geothermal field, to investigate the effectiveness of injecting a high pH solution with chelating agent. An industry-government cost-shared project at Desert Peak is underway to evaluate the technical feasibility of developing an Enhanced Geothermal System. The project is supported by US DOE, co-sponsored by Ormat Nevada, Inc., and is technically coordinated by GeothermEx, Inc.

2. Calcite Dissolution Using Chelating Agents

Removal of calcite scaling from wellbores is commonly accomplished by injecting strong mineral acids, such as HCl. Injected strong acid tends to enter the formation via the first fluid entry zone, dissolving first-contacted minerals aggressively while leaving much of the rest of the wellbore untreated.

An alternative to mineral acid treatments is the use of chelating agents such as ethylenediaminetetraacetic acid (EDTA) or nitrilotriacetic acid (NTA). Mella et al. (2006) performed laboratory experiments using EDTA and NTA to investigate the effectiveness of chelating agents for calcite dissolution in the formation. A laboratory reactor was designed and fabricated for investigating calcite dissolution using these agents under controlled conditions that simulate a geothermal reservoir. The setup and results will be discussed in the next section. Preliminary experimental data indicated that

both EDTA and NTA are effective dissolution agents, and that dissolution capacity increases with temperature.

Such agents have the ability to chelate (or bind) metals such as calcium. Through the process of chelation, calcium ions would be solvated by the chelating agent, driving calcite dissolution. The kinetics of calcite dissolution using chelating agents are not as fast as those using strong mineral acids. The lower dissolution rate allows the chelating agent to take a more balanced path through the formation and more evenly dissolve calcite in all available fractures, rather than following the first fluid entry zone and leaving the rest relatively untouched.

The structures of the two chelating agents in anionic form are shown in Figure 1. In the calcite chelating process, one $EDTA^{4-}$ molecule will first associate with two Ca^{2+} ions,

$$EDTA^{4-} + 2Ca^{2+} = Ca_2EDTA \quad (1a)$$

The decrease in Ca^{2+} concentration drives calcite dissolution:

$$calcite = Ca^{2+} + CO_3^{2-} \quad (1b)$$

By summing Eq. (1a) and (1b)×2, we have:

$$EDTA^{4-} + 2calcite = Ca_2EDTA + 2CO_3^{2-} \quad (1)$$

Theoretically one mole of $EDTA^{4-}$ can dissolves two moles of calcite. Similarly, two moles of NTA^{3-} can complex with three moles of Ca^{2+} ions,

$$2NTA^{3-} + 3Ca^{2+} = Ca_3NTA_2 \quad (2a)$$

By combining Eq. (2a) and (1b), we have:

$$2NTA^{3-} + 3calcite = Ca_3NTA_2 + 3CO_3^{2-} \quad (2)$$

Eq. (2) indicates that two moles of NTA^{3-} can dissolves three moles of calcite.

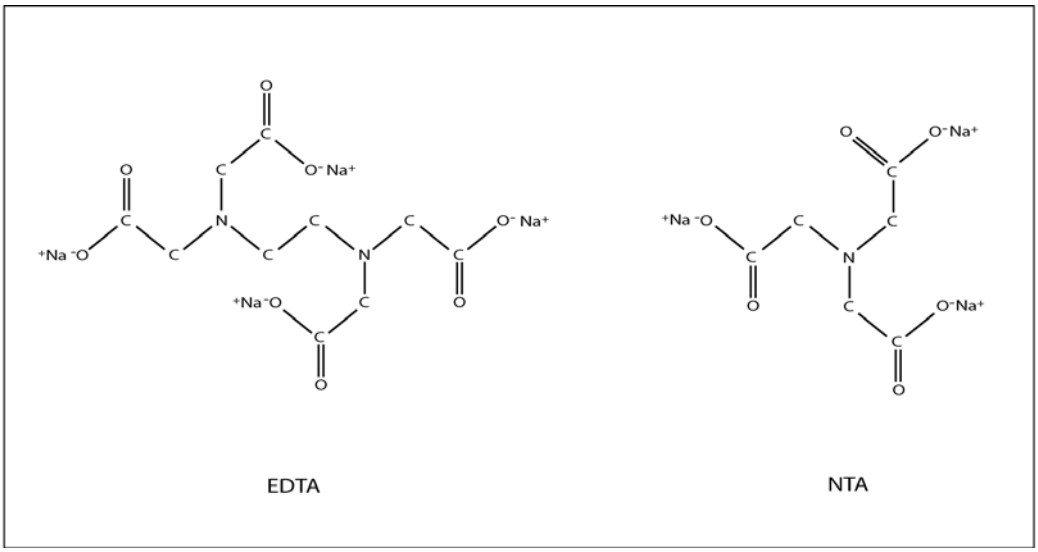

Figure 1. Chemical structures of the sodium salts of EDTA and NTA.

3. Numerical Modeling Method

3.1 General Features

The modeling of the laboratory experiment and field example was done with the non-isothermal reactive geochemical transport program TOUGHREACT, whose physical and chemical process capabilities and solution techniques have been discussed by Xu and Pruess (2001) and Xu et al. (2006). The program uses integral finite differences for space discretization (IFD; Narasimhan and Witherspoon, 1976). The IFD method provides for flexible discretization using irregular grids, which is well suited for modeling of flow, transport, and fluid-rock interaction in heterogeneous and fractured rock systems with varying petrology and complex model boundaries due to the presence of engineered structures. For regular grids, the IFD method is equivalent to the conventional finite difference method. An implicit time-weighting scheme is used for modeling flow, transport, and kinetic geochemical reactions.

The program can be applied to one-, two-, or three-dimensional porous and fractured media with physical and chemical heterogeneity, and can accommodate any number of chemical species present in liquid, gas and solid phases. A broad range of subsurface thermal-physical-chemical processes is considered under various thermohydrological and geochemical conditions of pressure, temperature, water

saturation, ionic strength, and pH and Eh. Temporal changes in porosity and permeability due to mineral dissolution and precipitation are considered in the model. Mineral dissolution and precipitation are considered under kinetic conditions. Changes in porosity are calculated from changes in mineral volume fractions. Several porosity-permeability relationships are considered in the simulator as discussed in Xu et al. (2004), including the cubic Kozeny-Carman grain model and the Verma-Pruess model (1988).

3.2 Reaction Kinetics

Kinetics of mineral dissolution are very important for chemical stimulation of an EGS reservoir. A general kinetic rate law for mineral dissolution and precipitation is used in TOUGHREACT (Lasaga et al., 1994),

$$r_n = \pm k_n A_n \left| 1 - \left(\frac{Q_n}{K_n} \right)^{\theta} \right|^{\eta} \tag{3}$$

where n denotes kinetic mineral index, positive values of r_n indicate dissolution, and negative values precipitation, k_n is the rate constant (moles per unit mineral surface area and unit time) which is temperature-dependent, A_n is the specific reactive surface area of the mineral, K_n is the equilibrium constant for the mineral-water reaction written for the destruction of one mole of mineral n, and Q_n is the reaction quotient. The parameters θ and η must be determined from experiments; usually, but not always, they are taken equal to one (like in the present work).

For many minerals, the kinetic rate constant k can be summed from three mechanisms (Lasaga et al., 1994; Palandri and Kharaka, 2004),

$$k = k_{25}^{nu} \exp\left[\frac{-E_a^{nu}}{R}\left(\frac{1}{T} - \frac{1}{298.15}\right)\right] + k_{25}^{H} \exp\left[\frac{-E_a^{H}}{R}\left(\frac{1}{T} - \frac{1}{298.15}\right)\right] a_H^{n_H} + k_{25}^{OH} \exp\left[\frac{-E_a^{OH}}{R}\left(\frac{1}{T} - \frac{1}{298.15}\right)\right] a_{OH}^{n_{OH}} \quad (4)$$

where superscripts or subscripts nu, H, and OH indicate neutral, acid and base mechanisms, respectively, E_a is the activation energy, k_{25} is the rate constant at 25°C, R is the gas constant, T is absolute temperature, a is the activity of the species; and n is an exponent (constant).

4. Model Calibration from Experimental Data

4.1. Experiment Setup

Laboratory experiments of calcite and silica dissolution using a high pH solution with NTA were performed by Rose et al (2008**,** unpublished data). The flow reactor used is shown in Figure 1. The reactor flow cell was 6 inches long with a 1-inch internal diameter. The top 3 inches (7.62 cm) were filled with calcite chunks (30 g limestone) and the bottom 3 inches with silicate glass beads (or amorphous silica or quartz for different experiments). Water was injected from the top of the reactor with a flow rate of 3.333×10^{-5} kg/s (2 ml/min). Experiments were conducted for a range of temperatures from 150 to 300^{o}C. The injection water was prepared by adding Na-NTA reagent and NaOH to distilled water (representing steam condensate), the resulting injection water had a NTA^{3-} concentration of 0.1 mol/kgw (w denotes H_2O), and a high pH. In the modeling a pH of 11.5 was used because the maximum value of pH decreases with temperature, the highest pH possible at 150^{o}C being 11.63, while at 300^{o}C it is 11.3. Measured total amounts of silica and calcite dissolved (in percent) after each experiment with six-hour duration are presented in Figures 3 and 4. Each data point represents one experiment at a constant temperature.

A 1-D model using TOUGHREACT was developed for the dissolution experiments described above. Experimental data were then compared to model outputs and model parameters were adjusted as necessary to match the data.

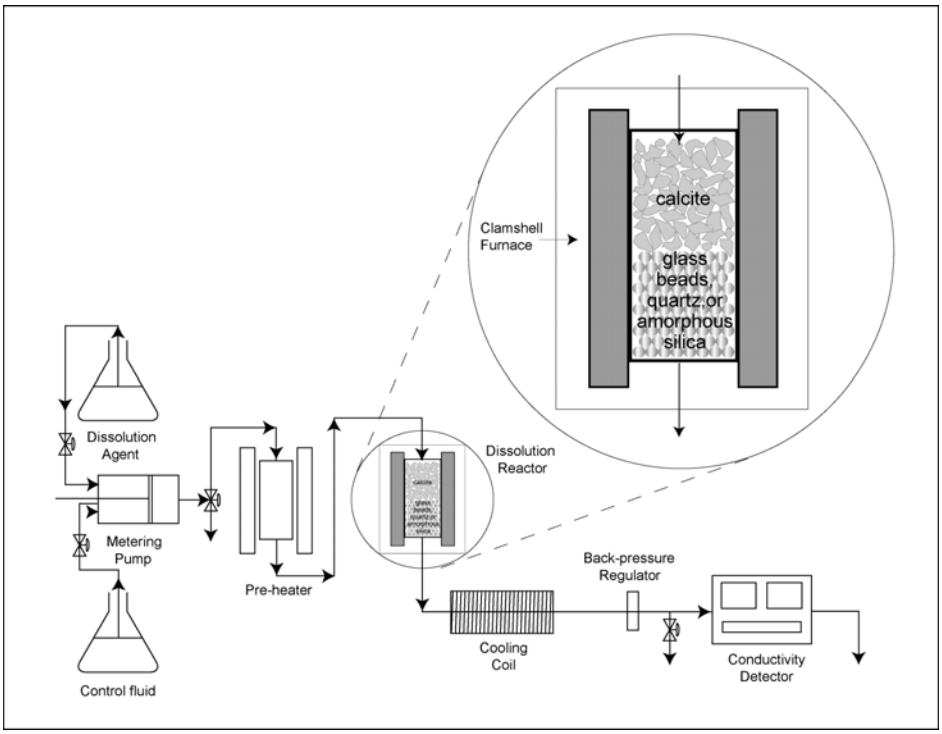

Figure 2. Schematic drawing of the high-temperature flow reactor.

4.2. Silica dissolution

For silica, the following expression was used in the calibration of the kinetic model for its dissolution,

$$r = Ak_{25} \exp\left[\frac{-E_a}{R}\left(\frac{1}{T} - \frac{1}{298.15}\right)\right]\left(1 - \frac{c}{K}\right) \quad (5)$$

where r is silica dissolution rate (moles per unit mineral surface area and per unit time, mol m^{-2} s^{-1}), and c is the dissolved silica (SiO_2) concentration (mol/kgw). Other parameters are the same as defined in Eqs. (3) and (4). Eq. (5) has only one mechanism,

which is a special case of the general multi-mechanism rate law defined in Eqs. (3) and (4).

The rate expression Eq. (5) has three parameters, A, k_{25}, and E_a, which are obtained by calibrating measured data of silica dissolution. In fact, only the product of A and k_{25} appears in Eq. (5). We used a reactive surface area of A = 98 cm^2 g^{-1}, which is calculated by assuming a cubic array of truncated spheres (Sonnenthal, 2005). Therefore, only k_{25} and E_a need to be calibrated for the silica dissolution rate model. The total amounts of silica dissolved in the model were matched to measurements by adjusting values of k_{25} and E_a (trial and error method), assuming that the dissolution rate is linear with time.

Three curves for different parameter values are presented together with measured data in Figure 3. Curve 1 has $k_{25} = 1.05\times10^{-8}$ mol m^{-2} s^{-1} and E_a = 39 kJ mol^{-1}, and fits well with measured amorphous silica dissolution data for temperature range from 160 to 250^{o}C. Curve 2 has $k_{25} = 1.85\times10^{-8}$ mol m^{-2} s^{-1} and E_a = 33.8 kJ mol^{-1}, and agrees with measured glass bead data for 160 to 220^{o}C temperatures. Curve 3 has $k_{25} = 1.14\times10^{-8}$ mol m^{-2} s^{-1} and E_a = 32.8 kJ mol^{-1}, and matches well with quartz dissolution data for 160-230^{o}C temperatures. Variations with temperature of the amount of silica dissolved are reflected by the activation energy term E_a.

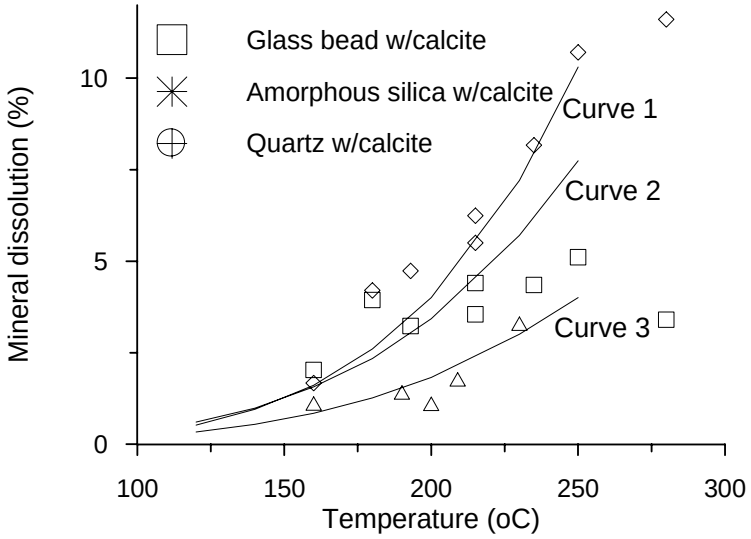

Figure 3. Measured total silica dissolution together with fitted models (curves).
Curve 1: $k_{25} = 1.05\times10^{-8}$ mol m^{-2} s^{-1}, $E_a = 39$ kJ mol^{-1};
Curve 2: $k_{25} = 1.85\times10^{-8}$ mol m^{-2} s^{-1}, $E_a = 33.8$ kJ mol^{-1};
Curve 3: $k_{25} = 1.14\times10^{-8}$ mol m^{-2} s^{-1}, $E_a = 32.8$ kJ mol^{-1}.

4.3. Calcite dissolution

Calcite is assumed to react with aqueous species at local equilibrium. Calcite dissolution is driven by the chelating processes as described above. For the example of an injection solution with NTA, the chelating reaction is given by Eq. (2) and is assumed to proceed according to a kinetic rate. A simple linear kinetic rate expression for formation of Ca_3NTA_2 was used,

$$r_{Ca} = k_{Ca} C_{NTA} \tag{6}$$

where r_{Ca} is the rate (mol kgw^{-1} s^{-1}), k_{Ca} is the rate constant (s^{-1}), C_{NTA} is NTA concentration (mol kgw^{-1}). As for the silica dissolution kinetic rates, we used an activation energy term k_{Ca} to describe the temperature-dependence,

$$k_{Ca} = k_{25}^{Ca} \exp\left[\frac{-E_a^{Ca}}{R}\left(\frac{1}{T} - \frac{1}{298.15}\right)\right] \quad (7)$$

Two parameters, k_{25}^{Ca} and E_a^{Ca}, are needed to calibrate the chelating process model (or calcite dissolution model). The total amounts of calcite dissolved in the model were matched to measurements by adjusting values of the two parameters. The fitted curve in Figure 4 has $k_{25}^{Ca} = 1.78\times10^{-4}$ s^{-1} and $E_a^{Ca} = 10$ kJ mol^{-1}.

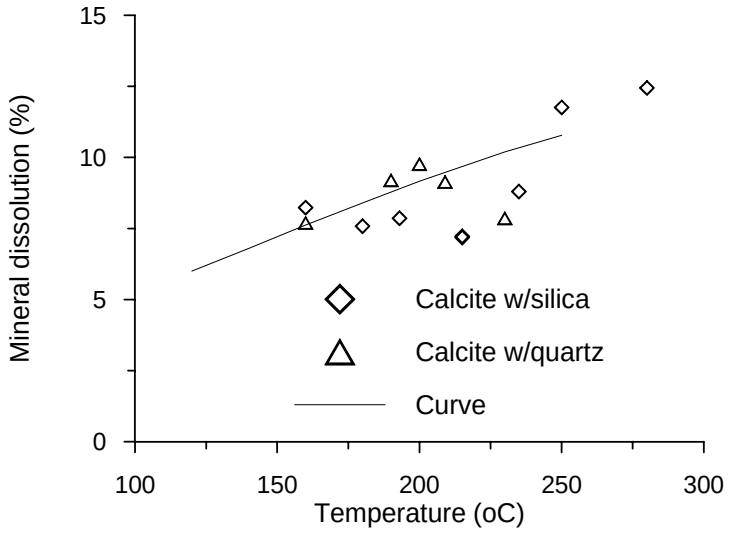

Figure 4. Measured total calcite dissolution together with the fitted model (curve).

Simulated aqueous concentrations along the column for the calibrated calcite dissolution model are presented in Figure 5. NTA^{3-} complexing with Ca^{2+} results in a decrease in its concentration and an increase in Ca_3NTA_2 concentration along the column. Ca^{2+} concentration remains low, maintaining calcite dissolution. Consequently dissolved carbon concentration increases continuously. Note that NTA^{3-} concentration was maintained constant at the inlet, and fluid velocity constant throughout the flow domain over time.

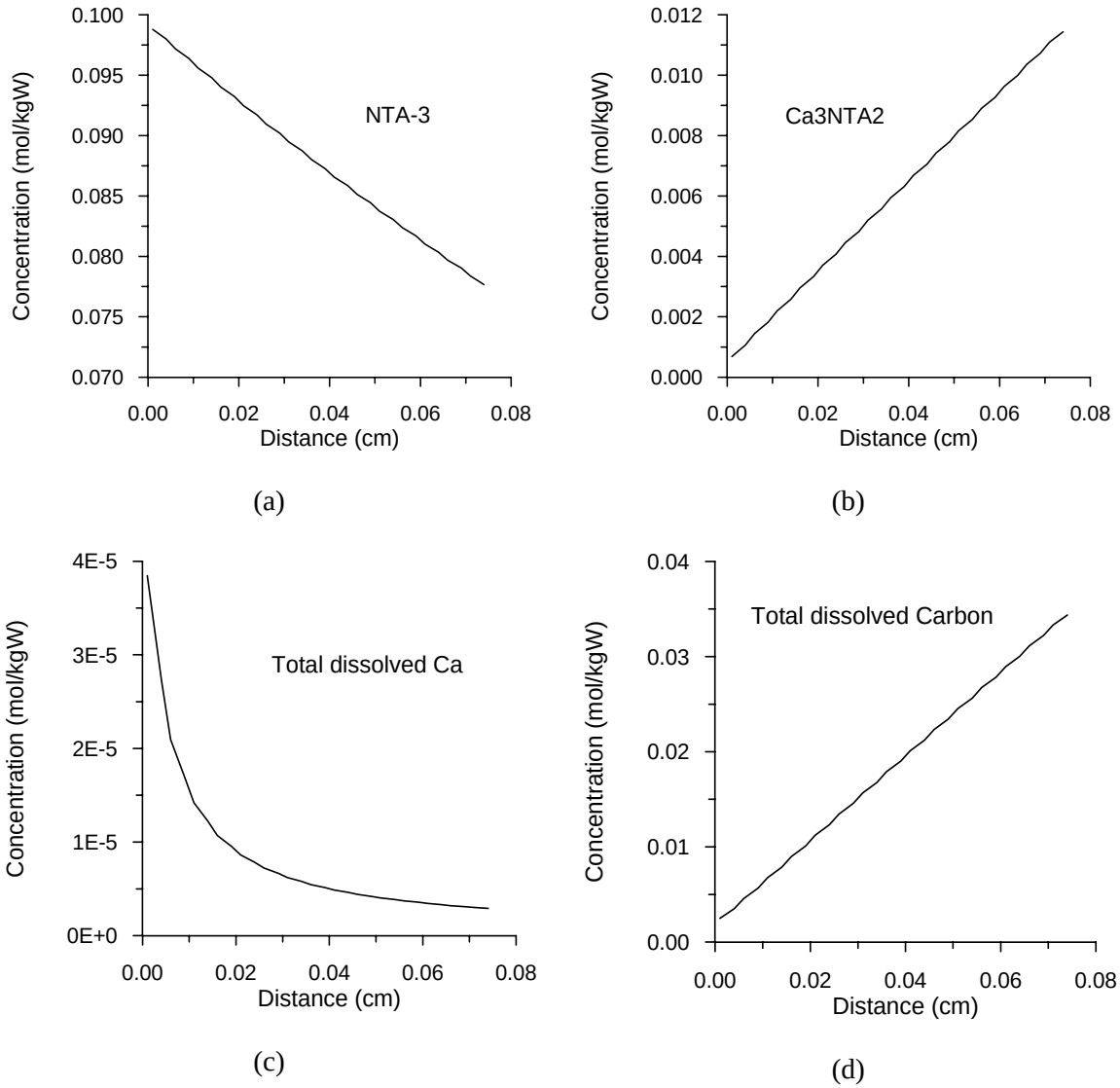

Figure 5. Simulated aqueous concentrations along the column for the calibrated calcite dissolution model.

5. Field Application

To investigate the effectiveness of injecting a high pH solution with chelating agent for the dissolution of calcite and silica minerals, we applied the model of chemical stimulation together with the calibrated parameters to a geothermal injection well system using a mineralogical composition from the Desert Peak (Nevada) geothermal field.

5.1. Model Setup

Geologic Setting and Mineralogy

In our model, the mineralogical composition was defined based on pre-Tertiary unit 2 (pT2) from well DP 23-1, which is a quartz monzodiorite with 7-10 wt % quartz, 40-45 wt% plagioclase, 10-15 wt % potassium feldspar and 1-4 wt % sphene. A plot of lithologies, secondary and hydrothermal alteration minerals, and measured subsurface temperatures for DP 23-1 is shown in Figure 6 (Benoit et al., 1982; Lutz et al., 2004). A clinopyroxene and hornblende-bearing diorite directly overlies the main granodiorite intrusive body. The diorite is medium crystalline and contains primary hornblende phenocrysts with cores of clinopyroxene. The diorite is strongly propylitically altered to epidote, chlorite, pyrite and calcite, is moderately sericitized, and has also been thermally metamorphosed by the underlying granodiorite intrusive.

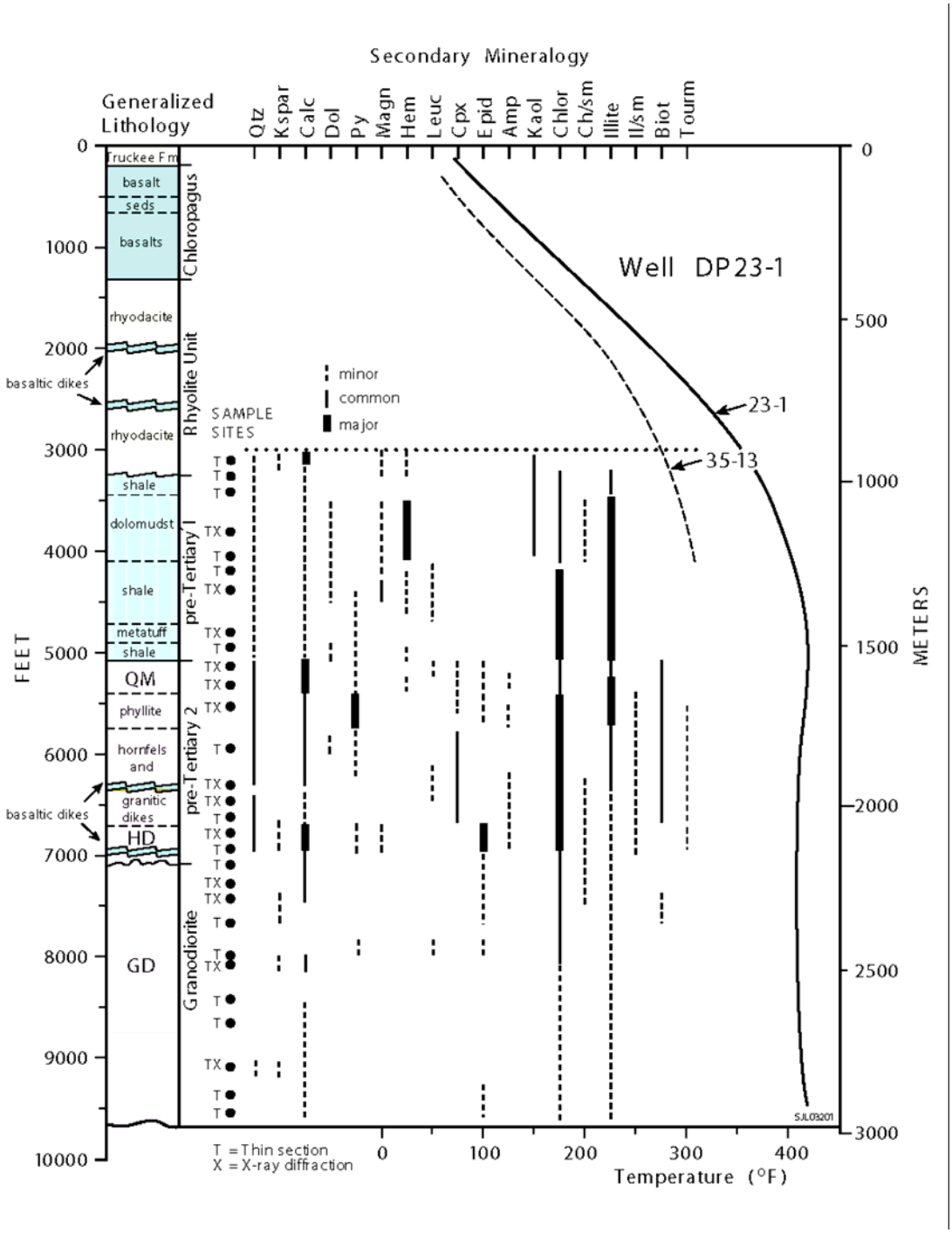

Figure 6. Lithologic column, distribution of secondary and hydrothermal alteration minerals in the pre-Tertiary section, and measured wellbore temperatures for well DP 23-1. Measured temperatures for core hole 35-13 TCH are also shown (Benoit et al., 1982; Lutz et al., 2004). Explanation - Mineral abundances: Major = 15-5-%; Common = 5-15%; Minor = 1-5%. Mesozoic intrusives: QM = Jurassic quartz monzodiorite; HB = Jurassic hornblende diorite; GD = Cretaceous granodiorite.

Initial mineralogical composition used in the modeling is summarized in Table 1. The compositions specified were based on the mineralogy of the crystalline rock along a fracture (Table 1; Figure 6). Plagioclase was modeled using 50% low-albite and 50% anorthite. Other minerals including epidote, pyrite, and biotite were not considered in the model, because their reactions with injection solution are slow and not important for the chemical stimulation purpose.

Table 1. Initial mineralogical compositions used in the numerical modeling.

Mineral	Quartz monzodiorite (% in terms of solid).
Quartz	9
Calcite	12
Low-Albite	21.5
Anorthite	21.5
K-Feldspar	13
Chlorite	8
Illite	7
Others	8

Reaction kinetics

Table 2 lists parameters for the kinetics of mineral reactions used in the model. For quartz, specific reactive surface area and kinetic parameters k_{25} and E_a were taken from the calibration of the laboratory experiment (Curve 3 of Figure 3). Specific reactive surface areas for low-albite, anorthite, and K-feldspar are set the same as for quartz. Surface area for chlorite and illite was from Sonnenthal et al. (2005), calculated assuming a cubic array of truncated spheres constituting the rock framework. The larger surface areas for these clay minerals are due to smaller grain sizes. Kinetic parameters k_{25} and E_a for low-albite, anorthite, K-feldspar kaolinite, chlorite, and illite were taken from Palandri and Kharaka (2004), who compiled and fitted experimental data reported by many investigators. The detailed list of the original data sources is given in Palandri and Kharaka (2004). Calcite dissolution is controlled by the kinetics of the chelating process and the calibrated parameters mentioned above were used.

The experimental data for quartz and calcite have substantial scatter over a range of temperatures 150-300^{o}C (Figures 3 and 4). In this modeling example, however, dissolution of both minerals mainly occurs near the injection well with a temperature close to 160^{o}C of the injection water (see results given below). Therefore the errors on the derived parameters propagate through the numerical simulation would be minimum.

Table 2. Parameters for calculating kinetic rate constants of minerals. Note that (1) all rate constants are listed for dissolution; (2) A is specific surface area, k_{25} is kinetic constant at 25°C, E_a is activation energy, and n is the exponent term (Eq. 4); (3) the exponent terms n for both acid and base mechanisms are with respect to H^+.

Mineral	*A* (cm^2/g)	*Parameters for kinetic rate law*							
		Neutral mechanism		*Acid mechanism*			*Base mechanism*		
		k_{25} ($mol/m^2/s$)	E_a (KJ /mol)	k_{25}	E_a	$n(H^+)$	k_{25}	E_a	$n(H^+)$
Quartz	98	1.14×10^{-8}	32.8						
Low-albite	98	2.754×10^{-13}	69.8	6.918×10^{-11}	65	0.457	2.512×10^{-16}	71	-0.572
Anorthite	98	2.754×10^{-13}	69.8	6.918×10^{-11}	65	0.457	2.512×10^{-16}	71	-0.572
K-feldspar	98	3.890×10^{-13}	38	8.710×10^{-11}	51.7	0.5	6.310×10^{-22}	94.1	-0.823
Chlorite	1516	3.02×10^{-13}	88	7.762×10^{-12}	88	0.5			
Illite	1516	1.660×10^{-13}	35	1.047×10^{-11}	23.6	0.34	3.020×10^{-17}	58.9	-0.4

Flow conditions

A 120 m thick reservoir formation with an injection well was modeled. A simple one-dimensional radial flow model was used, consisting of 50 radial blocks with logarithmically increasing radii out to a distance of 1000 m from the wall of the drilled open hole (Figure 7). Only the fracture network is considered in the model, with the assumption that the fluid exchange with the surrounding low permeability matrix is insignificant for the short period of chemical stimulation. An initial fracture permeability of 5.2×10^{-12} m^2 was assumed. A fracture porosity of 1% (ratio of fracture volume to the total formation volume) was assumed. The 1% volume of wall rock was included in the fracture domain, to allow minerals on the fracture walls to interact chemically with injection water. Therefore, a fraction of 2% of total volume was included in the fracture domain, with an initial porosity of 0.5, and a permeability of 2.6×10^{-12} m^2. The uncertainty on the permeability specification doesn't affect modeling results of reactive

transport and porosity enhancement (as long as pressure buildup at the wellbore can be afforded) because a constant injection rate was specified in the present study.

Conductive heat exchange with rocks of low permeability above and below this zone is an important process when injection temperature differs from the reservoir temperature. The confining layers are modeled as semi-infinite half spaces, and heat exchange is treated with a semi-analytical technique due to Vinsome and Westerveld (1980). Initial reservoir temperature is 210°C as indicated in Figure 6. An initial hydrostatic pressure of 20 MPa was assumed for about 2000 m depth. Hydrogeologic specifications of the 1-D radial flow problem are given in Table 3.

Two injection temperatures of 120 and 160°C were used (details will be discussed below). Injection water chemistry was the same as in the modeling of laboratory experiments, which was prepared by adding NTA agent and NaOH solution to steam condensate, and had a NTA^{3-} concentration of 0.1 mol/kgw, a Na^{+} concentration of 1.5 mol/kgw, and a pH of 11.5. The initial water chemistry is in equilibrium with the initial mineralogy at a reservoir temperature of 210^{o}C. An injection rate of 10 kg/s was applied for a period of half a day. Reactive transport simulations were performed for a total time of one day, including a no-flow period after the 12-hour injection.

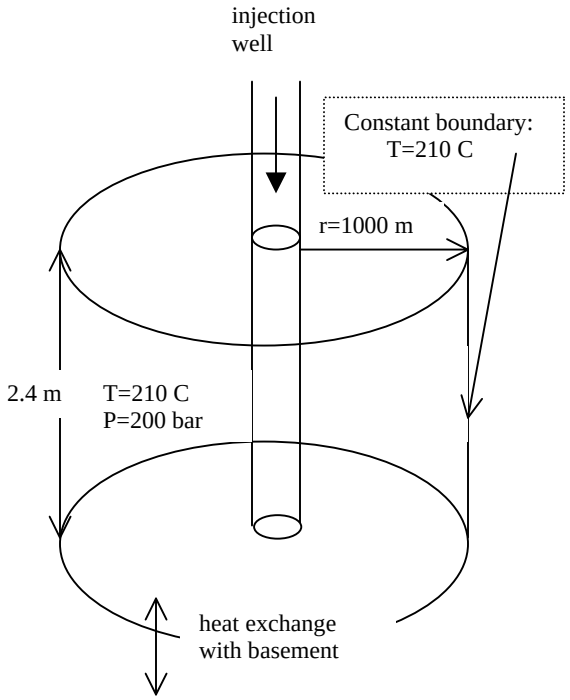

Figure 7. Simplified conceptual model for 1-D radial flow around a geothermal injection well.

Table 3. Geometric and hydrogeologic specifications for 1-D radial flow problem.

Reservoir properties:	
Permeability	2.6×10^{-12} m^2
Porosity	0.5
Rock grain density	2750 kg m^{-3}
Rock specific heat	1000 J kg^{-1} ^{o}C^{-1}
Thermal conductivity	2.4 W m^{-1} ^{o}C^{-1}
Initial and boundary conditions:	
Pressure	200 bar
Temperature	210^{o}C
Injection conditions (base case):	
Temperature	160^{o}C
Rate	10 kg s^{-1}
Duration	12 hours

Simulation setup

A total of four simulations were performed (Table 4). We started with a simulation using an injection water temperature of 160^{o}C (base-case). Many chemical and thermophysical factors affect mineral dissolution and associated enhancement in formation porosity and permeability, including mineral abundance and distribution in the formation, and injection temperature and rate, and reaction kinetics. Therefore, in the second simulation, we used a lower temperature of 120^{o}C. Other conditions and parameters are the same as in the base-case. In Simulation 3, the injection rate was increased to 30 kg/s from 10 kg/s in the base-case. In Simulation 4, the reaction rate constants for all mineral and chelating reactions were decreased by a factor of 5.

The evolution of reaction rate and the reactive surface area of a mineral are very complex, especially for multi-mineral systems, and is not quantitatively understood at present. The magnitudes of surface areas specified are highly uncertain. Aqueous solution interaction with the minerals in the field is generally expected to occur only at selective sites of the mineral surface, and the actual reactive surface area could be between one and three orders of magnitude less than the geometric surface area (Lasaga, 1995; Zerai et al. 2006). The difference is attributed to the fact that only part of the mineral surface is involved in the reaction due to coating or armoring, a small area exposed to water, and channeling of the reactive fluid flow.

Table 4. List of simulations performed with different specifications.

Simulation	Specification
1. Base-case	160^{o}C injection
2. Low temperature	120^{o}C injection
3. Large injection rate	Injection rate increased by three times to 30 kg/s
4. Low reaction rate	Rate constant reduced by a factor of 5

5.2. Results and Discussion

Injection of the high pH solution with chelating agent (NTA) results in increases in porosity along the flow path close to the injection well. Porosity profiles at different times obtained for four cases are presented in Figure 8. Increases in porosity are mainly caused by dissolution of calcite, low-albite and anorthite (Figures 9, 11, and 12). In the base-case with an injection temperature of 160^{o}C, the porosity increases to 60% from an initial value of 50% close to the injection point; enhancement of porosity extends to a radial distance of about 5 m (Figure 8a). A low temperature injection (120^{o}C) results in a smaller porosity increase (to 56%) close to the injection point, but a longer extent to a radial distance of about 7 m (Figure 8b). For Case 3 with injection rate increased by three times, the porosity increases to 61% close to the injection point, and the enhancement extends to a longer distance of about 8 m (Figure 8c). Reduction of reaction rate (Case 4) results in less dissolution close to the injection point and to a larger extent along the flow path (compare Figure 8d to 8a), indicating that smaller reaction rates may be more effective for chemical stimulation.

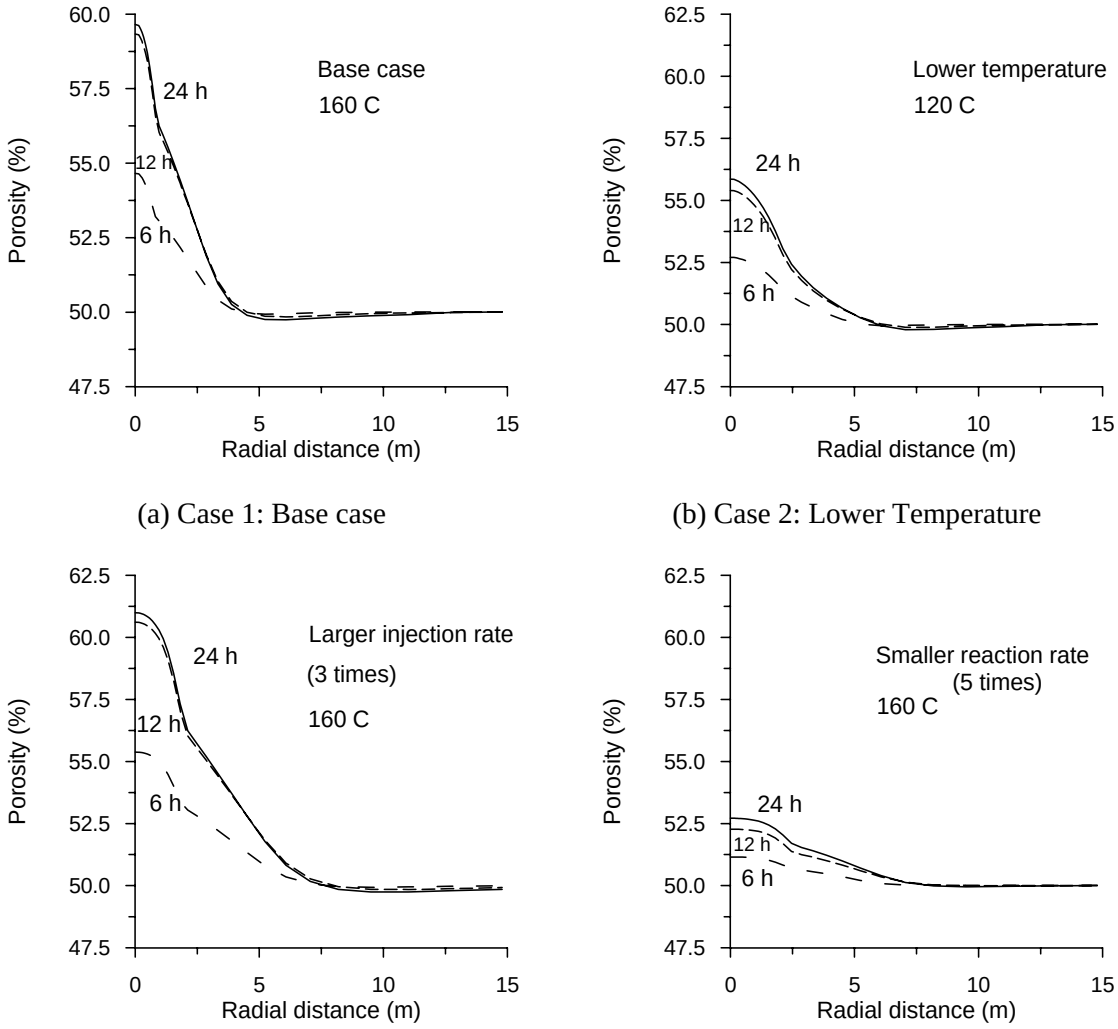

(a) Case 1: Base case

(b) Case 2: Lower Temperature

(c) Case 3: Larger injection rate

(d) Case 4: Smaller reaction rate

Figure 8. Porosity profiles at different times obtained for the four cases (Initial porosity of the fracture domain is 50%).

Now we discuss the dissolution of individual minerals along the flow path. A decrease in injection temperature from 160 to 120^{o}C results in no significant changes in the calcite dissolution pattern, with a maximum dissolution of 3.6% close to the injection point (compare Figure 9b to 9a). A larger injection rate produces a slightly higher calcite dissolution (4.5%) close to the injection point, and the dissolution extends to a much longer distance of more than 5 m (Figure 9c). For the first three cases, small amounts of

precipitation occur at the moving thermal front because an increase in temperature causes a decrease in calcite solubility. A reduction in reaction rate causes a reduction of calcite dissolution (1%) close to the injection point, dissolution extends to a larger distance of about 6 m, and no precipitation of calcite occurs at the moving thermal front (Figure 9d). For all four cases, the amounts of quartz dissolution are very small because of a small reaction rate (Figure 10). Generally low-albite dissolves close to the injection point due to high pH, but precipitates along the flow path because of lowered pH and high injected Na^+ concentration (Figure 11). Anorthite dissolves along the flow path because of low Ca^{2+} concentration (Figure 12). K-feldspar, chlorite, and illite all dissolve close to the injection point and precipitate later along the flow path, but the amounts of their dissolution and precipitation are very small.

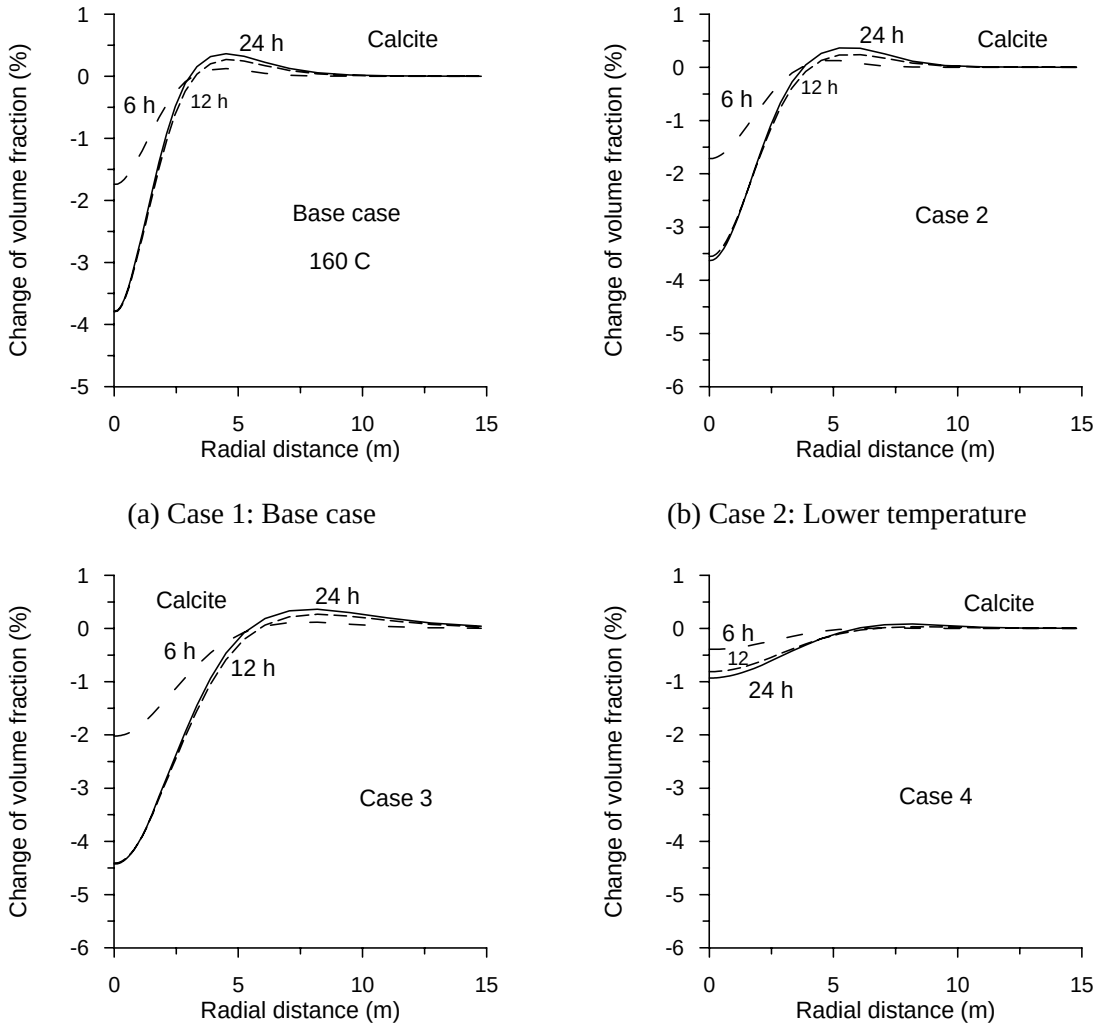

(a) Case 1: Base case

(b) Case 2: Lower temperature

(c) Case 3: Larger injection rate

(d) Case 4: Smaller reaction rate

Figure 9. Changes of calcite abundance (in percentage of volume fraction, negative values indicate dissolution, positive precipitation) at different times for the four cases.

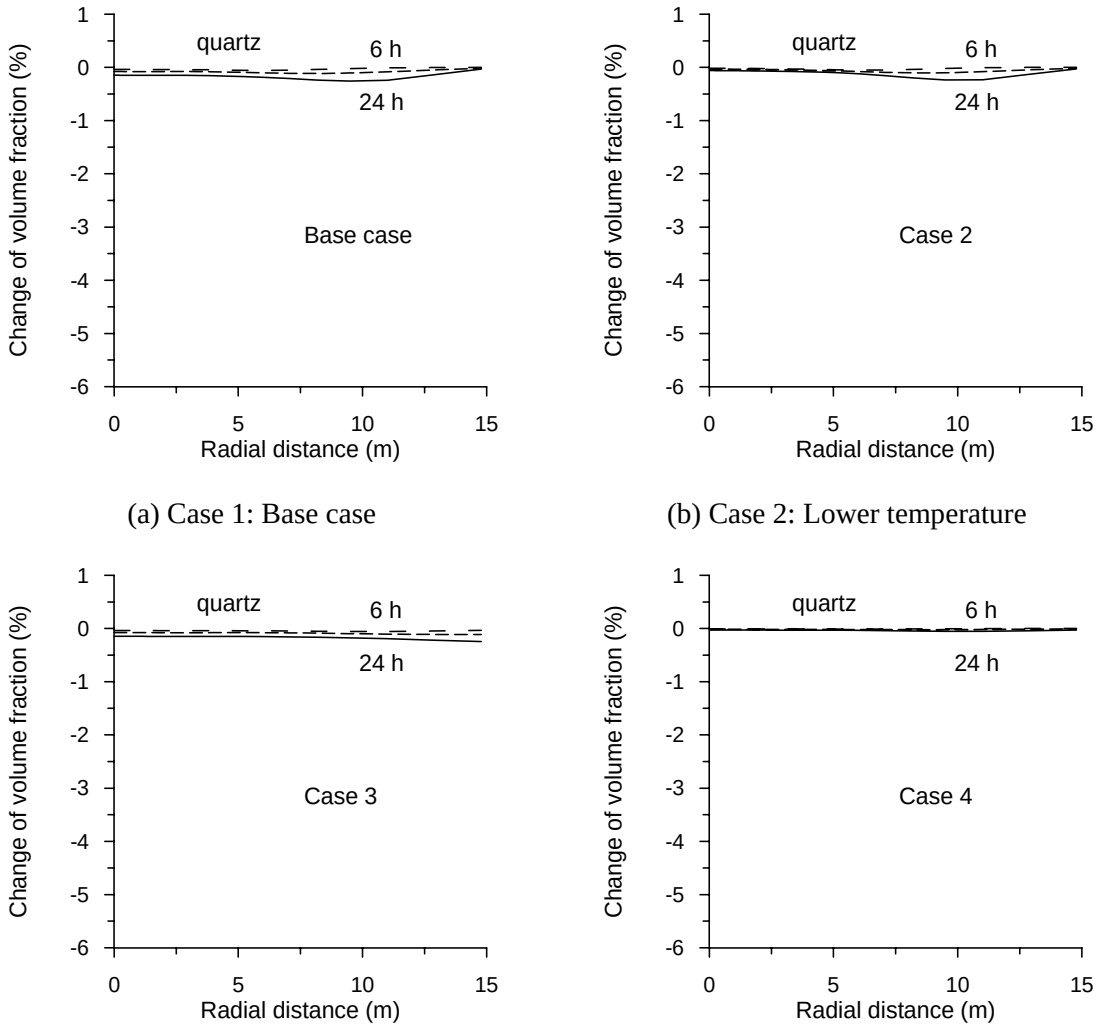

(a) Case 1: Base case

(b) Case 2: Lower temperature

(c) Case 3: Larger injection rate

(d) Case 4: Smaller reaction rate

Figure 10. Changes of quartz abundance (in percentage of volume fraction) at different times for the four cases.

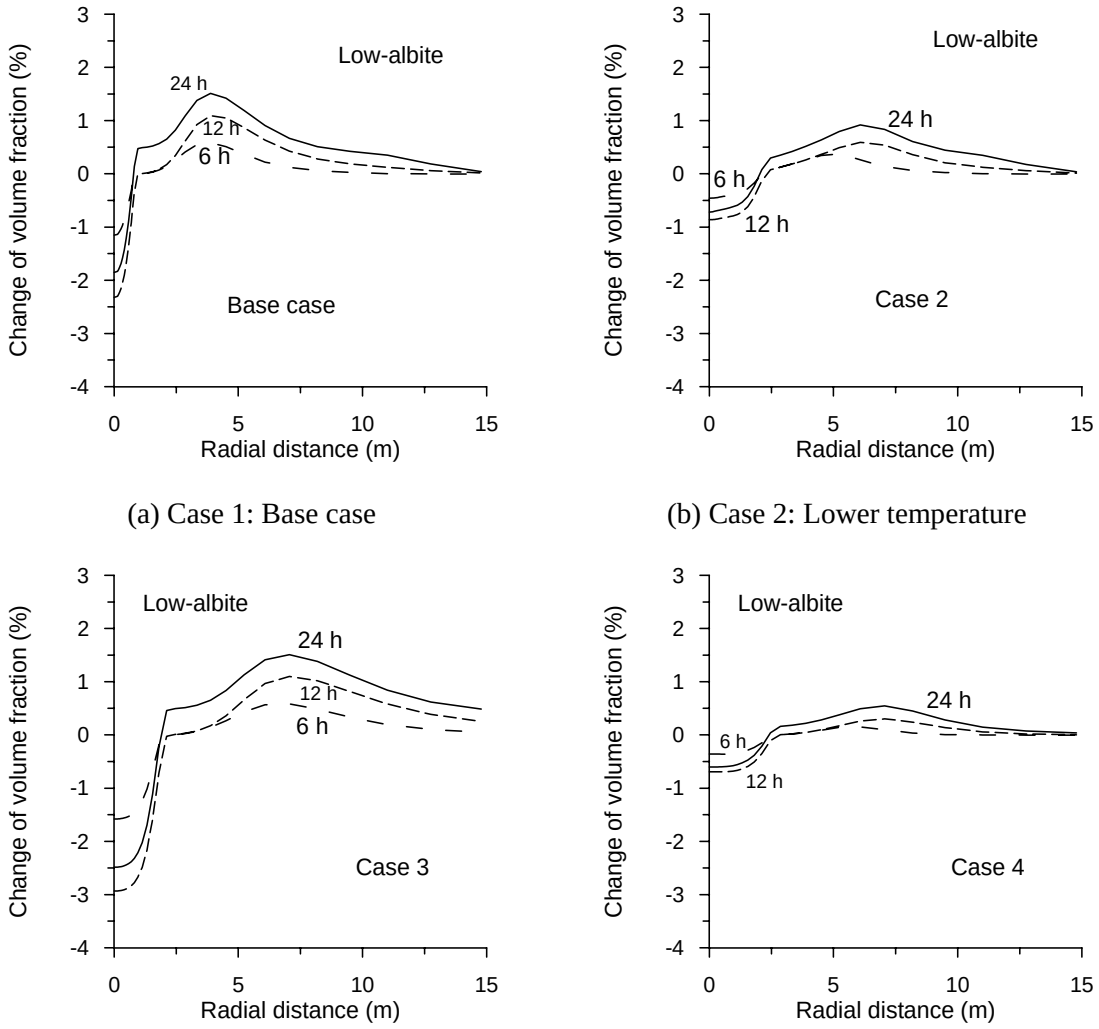

(a) Case 1: Base case

(b) Case 2: Lower temperature

(c) Case 3: Larger injection rate

(d) Case 4: Smaller reaction rate

Figure 11. Changes of low-albite abundance (in percentage of volume fraction, negative values indicate dissolution, positive precipitation) at different times for the four cases.

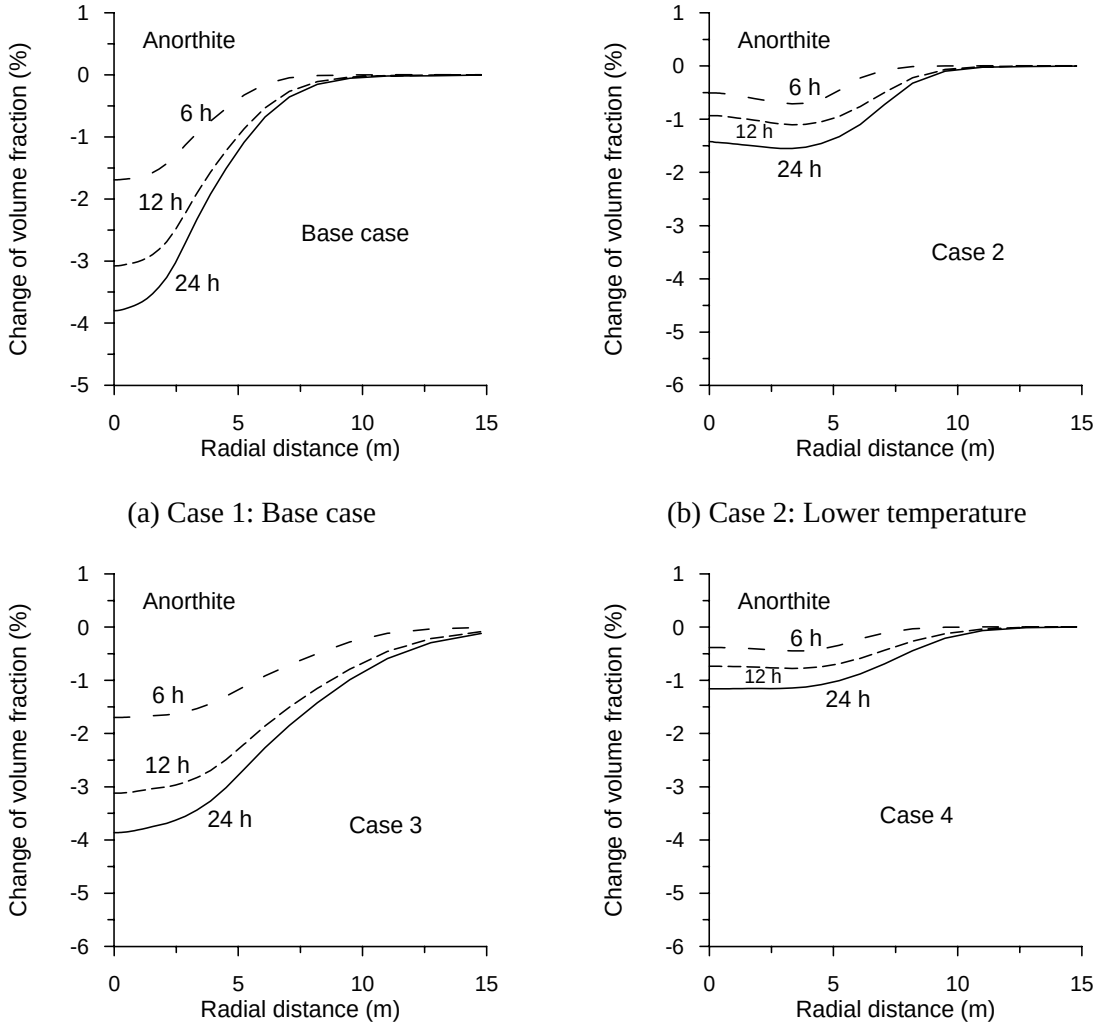

(a) Case 1: Base case

(b) Case 2: Lower temperature

(c) Case 3: Larger injection rate

(d) Case 4: Smaller reaction rate

Figure 12. Dissolution of anorthite (in percentage of volume fraction) at different times for the four cases.

Profiles of temperature, aqueous concentrations, and pH distribution (Figure 13) for the base-case simulation are examined next. Temperature reaches the initial value of 210°C after 12 hours at a distance of about 13 m for the 10 kg s^{-1} injection rate (Figure 13a). NTA^{3-} concentration increases during the 12-hour injection period (Figure 13b). After injection stops, NTA^{3-} is continuously complexing with Ca^{2+} and driving calcite dissolution, its concentration decreases, and it is used up at 24 hours. Total dissolved carbon concentrations (mainly CO_3^{2-}) increase gradually along the flow path because of

calcite dissolution (Figure 13c), and reach a maximum at the calcite dissolution front. The distribution of pH is controlled by the injection pH, consumption of OH^- by silica/silicate mineral dissolution, and transport processes (Figure 13d).

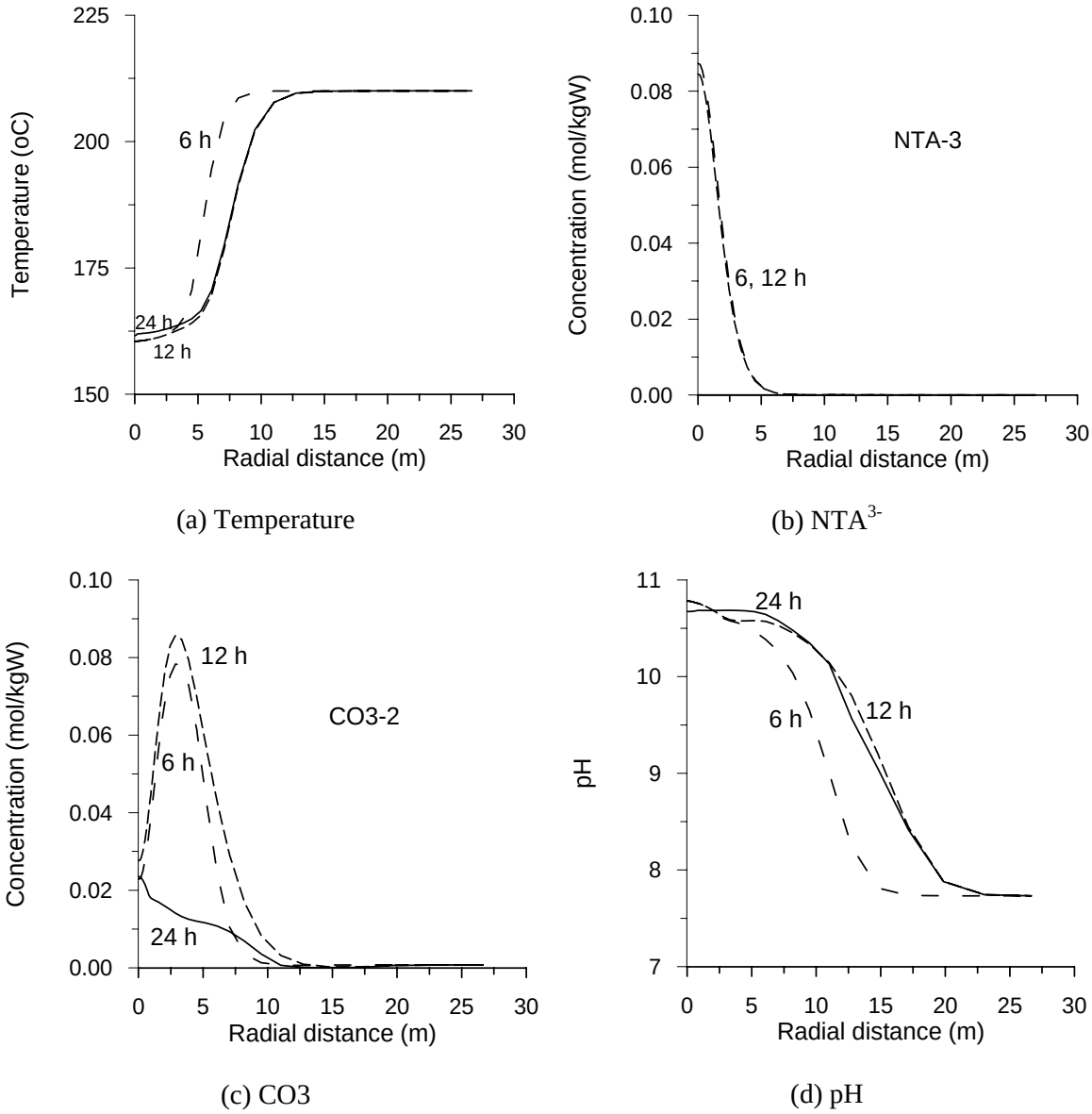

(a) Temperature (b) NTA^{3-}

(c) CO3 (d) pH

Figure 13. Profiles of temperature, NTA^{3-}, dissolved carbon concentrations, and pH at different times obtained for the base-case with an injection temperature of 160°C.

6. Summary and Conclusions

Dissolution of silica and calcite minerals in the presence of a chelating agent (NTA) at high pH was successfully demonstrated in the laboratory using a high-temperature flow reactor. The mineral dissolution and associated porosity enhancement in the laboratory experiment was reproduced by reactive transport modeling using TOUGHREACT, resulting in calibrated parameters for a dissolution model of calcite and silica minerals. The chemical stimulation method together with calibrated parameters was applied by numerical modeling to a field geothermal injection well system. Parameters applicable to a crystalline quartz monzodiorite rock unit at the Desert Peak EGS site were used. The following conclusions can be drawn from the numerical experiments.

The injection of a high pH chelating solution (NTA) results in dissolution of both calcite and plagioclase minerals, while avoiding precipitation of calcite at high temperatures. Consequently reservoir porosity and permeability can be enhanced in a region extending several meters around the injection well. A lower temperature injection results in a smaller porosity increase close to the injection point, but a greater extent further into the formation. Increase in injection rate causes a larger extent of mineral dissolution, favorable for chemical stimulation. Decrease in reaction rate results in less aggressive dissolution close to the injection point and larger extent along the flow path. More detailed investigations will be conducted in the future when data will become available from EGS field demonstration projects.

Acknowledgements. The first and fourth authors (Tianfu Xu and Karsten Pruess) were supported by the Assistant Secretary for Energy Efficiency and Renewable Energy, Office of Geothermal Technologies, of the U.S. Department of Energy, under Contract No. DE-AC02-05CH11231. The second and third authors (Peter Rose and Scott Fayer) were supported by the same Agency under grant DE-FG36-04GO14295.

References

Benoit, W.R., J.E. Hiner, and R.T Forest, 1982. Discovery and geology of the Desert Peak Geothermal Field: A case history, Nevada Bureau of Mines and Geology Bulletin 97, 82p.

Lasaga, A.C., Soler, J.M., Ganor, J., Burch, T.E., Nagy, K.L., 1994. Chemical weathering rate laws and global geochemical cycles. Geochimica et Cosmochimica Acta, 58, 2361-2386.

Lasaga, A.C., 1995. Fundamental approaches in describing mineral dissolution and precipitation rates. In: White, A.F., Brantley, S.L. (Eds.), Chemical Weathering Rates of Silicates Minerals, Reviews in Mineralogy, vol. 31. BookCrafters, Chelsea, MI, pp. 23–86.

Lutz, S.J., A.R. Tait, and C.L. Morris, 2004. Stratigraphic relationships in mesozoic basement rocks at the Desert Peak east EGS area, Nevada, In Proceedings of Twenty-Ninth Workshop on Geothermal Reservoir Engineering, Stanford University, Stanford, California.

Mella, M., Kovac, K., Xu, T., Rose, P., Mcculloch, J., Pruess, K., 2006. Calcite dissolution in geothermal reservoirs using chelants, In Proceedings of Geothermal Resources Council.

MIT, 2006. The future of geothermal energy impact of enhanced geothermal systems (EGS) on the United States in the 21st Century. A report for the U.S. Department of Energy, Massachusetts Institute of Technology.

Narasimhan, T.N., Witherspoon, P.A., 1976. An integrated finite difference method for analyzing fluid flow in porous media, Water Resour. Res. 12, 57–64.

Palandri, J., Kharaka, Y.K., 2004. A compilation of rate parameters of water-mineral interaction kinetics for application to geochemical modeling. US Geol. Surv. Open File Report 2004-1068, 64 pp.

Rose, P., T. Xu, K. Kovac, M. Mella, and K. Pruess, 2007. Chemical stimulation in near-wellbore geothermal formations: silica dissolution in the presence of calcite at high temperature and high pH, In Proceedings of Thirty-Second Workshop on Geothermal Reservoir Engineering, Stanford University, Stanford, California, January 22-24, 2007.

Sonnenthal E., Ito, A., Spycher, N., Yui, M., Apps, J., Sugita, Y., Conrad, M., Kawakami, S., 2005, Approaches to modeling coupled thermal, hydrological, and chemical processes in the Drift Scale Heater Test at Yucca Mountain. *International Journal of Rock Mechanics and Mining Sciences*, 42, 6987-719.

Vinsome, P. K. W., and Westerveld, J., 1980. A simple method for predicting cap and base rock heat losses in thermal reservoir simulators. J. Canadian Pet. Tech., 19 (3), 87–90.

Verma, A. Pruess, K., 1988. Thermohydrological conditions and silica redistribution near high-level nuclear wastes emplaced in saturated geological formations: *Journal of Geophysical Research*, 93, 1159-1173.

Xu, T., and Pruess, K., 2001. Modeling multiphase non-isothermal fluid flow and reactive geochemical transport in variably saturated fractured rocks: 1. Methodology. Am. J. Sci., 301, 16-33.

Xu, T., Ontoy, Y. Molling, P., Spycher, N., Parini, M., Pruess, K., 2004. Reactive transport modeling of injection well scaling and acidizing at Tiwi Field, Philippines. *Geothermics*, v. 33(4), p. 477-491.

Xu, T., Sonnenthal, E.L., Spycher, N., Pruess, K., 2006. TOUGHREACT - A simulation program for non-isothermal multiphase reactive geochemical transport in variably saturated geologic media: Applications to geothermal injectivity and CO_2 geological sequestration, *Computer & Geoscience*, v. 32/2 p. 145-165.

Zerai , B., Saylor, B.Z., Matiso, G., 2006. Computer simulation of CO_2 trapped through mineral precipitation in the Rose Run Sandstone, Ohio. Applied Geochemistry, 21, 223-240.